Electronic Supplementary Material (ESI) for Materials Chemistry Frontiers.

Electronic Supplementary Information

TADF emitters based on a tri-spiral acridine donor and a spiro-*B*-heterotriangulene acceptor exhibiting high horizontal dipole orientation and high efficiencies in deep-blue OLEDs

Young Hoon Lee,[†a,c] Jeoungmin Ji,[†b] Thi Quyen Tran,[a] Taehwan Lee,[a] Jaehoon Jung,[a] Youngil Lee,*[a,c] Seunghyup Yoo,*[b] and Min Hyung Lee*[a]

[a] Department of Chemistry, University of Ulsan, Ulsan 44776, Republic of Korea

[b] School of Electrical Engineering, KAIST, Daejeon 34141, Republic of Korea

[c] Chemical Industry Research Institution, University of Ulsan, Ulsan, 44776, Republic of Korea

* E-mail: nmryil@ulsan.ac.kr; syoo.ee@kaist.edu; lmh74@ulsan.ac.kr

General Considerations

All operations were performed under an inert nitrogen atmosphere using standard Schlenk and glovebox techniques. Anhydrous-grade solvents (Aldrich) were dried over activated molecular sieves (5Å). Spectrophotometric-grade toluene was used as received from Merck. Commercial reagents were used without further purification after purchase. 1-Bromo-2-phenoxybenzene,[1] *tert*-butyl (2-bromophenyl)(phenyl)carbamate,[2] 10*H*-dispiro[acridine-9,9'-anthracene-10',9''-thioxanthene] (S-tsACH, **2e**),[3] and 2-bromo-4,4,12,12-tetramethyl-4,12-dihydro-3a^2-boraspiro[dibenzo[*cd,mn*] pyrene-8,9'-fluoren]-1,3,3a^1(12a),4a,4a^1(7a),6,8a,9,11-nonaene (Br-BAsBP)[4] were synthesized according to the reported procedures. Deuterated solvents from Eurisotop were used. NMR spectra were recorded on a Bruker AVANCE III HD 400 (400.13 MHz for ^{1}H, 100.61 MHz for ^{13}C, 128.38 MHz for ^{11}B) spectrometer at ambient temperature. Chemical shifts are given in ppm, and are referenced against external Me_4Si (^{1}H, ^{13}C) and $BF_3{\cdot}OEt_2$ (^{11}B). Mass spectra were obtained using a JEOL JMS700 high-resolution EI-mass spectrometer (HR EI-MS) at the Korea Basic Science Institute, Daegu, Korea. Elemental analyses were performed on a Flash 2000 elemental analyzer (Thermo Scientific). Thermogravimetric analysis (TGA) was performed with a TA Instruments Q50 under an N_2 atmosphere at a heating rate of 10 °C/min. Cyclic voltammetry experiments were carried out using a CHI600E system system.

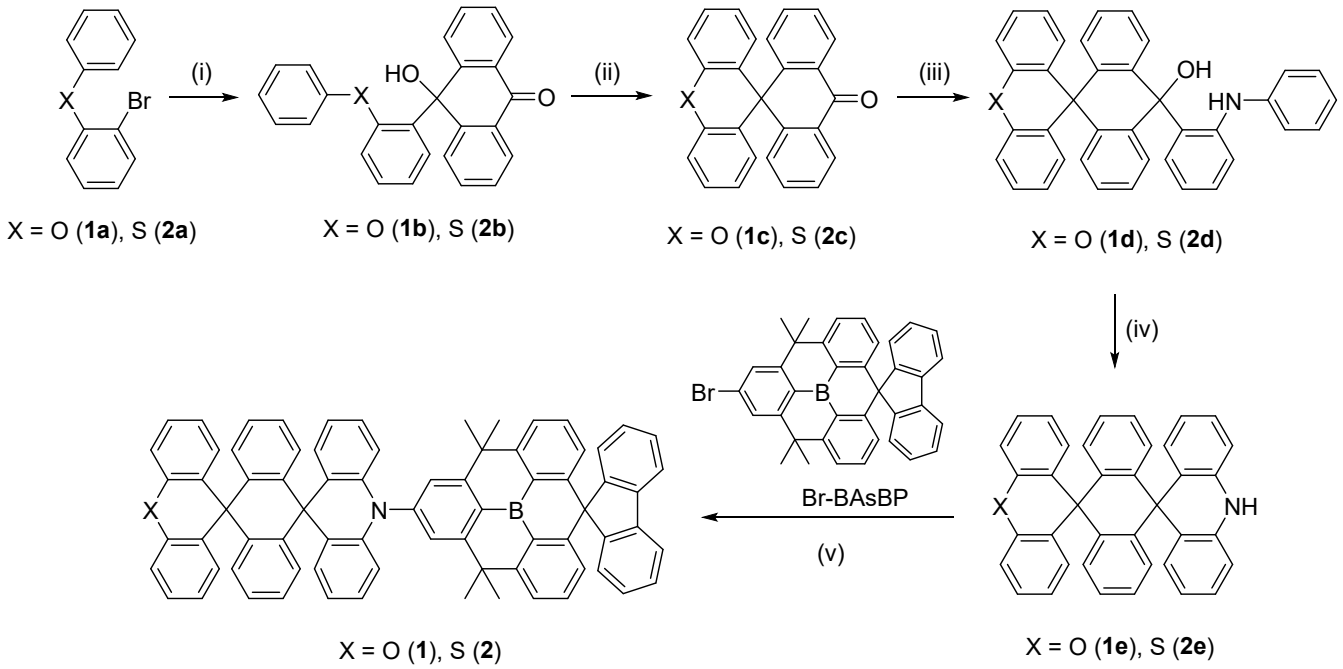

Reaction conditions: (i) *n*-BuLi, THF, −78 °C, then 1.0 M HCl, MeOH, RT. (ii) c-HCl, AcOH, reflux. (iii) *n*-BuLi, THF, −78 °C, then 1M HCl, MeOH, RT. (iv) c-HCl, AcOH, reflux. (v) Pd(*t*-$Bu_3P)_2$, Br-BAsBP, *t*-BuONa, toluene, reflux.

Synthesis of 10-hydroxy-10-(2-phenoxyphenyl)anthracen-9(10*H*)-one (1b)

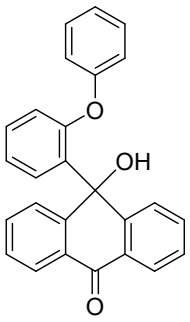

To a solution of 1-bromo-2-phenoxybenzene (1.1 g, 4.42 mmol) in dry THF (15 mL) was added dropwise *n*-BuLi (2.5 M in *n*-hexane, 1.8 mL, 4.50 mmol) at −78 °C. The reaction mixture was stirred for 1 h at −78 °C, then anthracene-9,10-dione (0.90 g, 4.32 mmol) in dry THF (10 mL) was slowly added at −78 °C. The reaction mixture was gradually allowed to warm to room temperature and stirred overnight. The mixture was quenched with methanol (5 mL), 1.0 M HCl (10 mL), and water (100 mL) in order. The reaction mixture was extracted with dichloromethane and the organic layer was dried over $MgSO_4$, filtered, and evaporated under reduced pressure. The crude product was purified by column chromatography on silica gel using diethyl ether/dichloromethane (1:2, *v/v*) as eluent. The eluate was concentrated under reduced pressure and recrystallized in dichloromethane/*n*-hexane to give **1b** as a pale yellow powder (Yield: 1.08 g, 68%) ^{1}H NMR ($CDCl_3$): δ 8.44 (dd, J = 7.8, 1.8 Hz, 1H), 8.10 (d, J = 8.0 Hz, 2H), 7.57–7.47 (m, 4H), 7.36–7.30 (m, 3H), 7.25 (td, J = 7.2, 1.6 Hz, 1H), 6.95 (t, J =7.2 Hz, 2H), 6.83 (tt, J = 7.6, 0.8 Hz, 1H), 6.61 (dd, J = 8.0, 1.2 Hz, 1H), 6.12–6.05 (m, 2H), 2.87 (s, 1H). ^{13}C NMR (CD_2Cl_2): δ 155.9, 152.2, 146.3, 137.2, 133.4, 130.2, 129.1, 128.9, 128.2, 127.8, 126.5, 126.1, 123.4, 122.5, 119.8, 117.0, 70.8. HRMS (EI): m/z Calcd for $C_{26}H_{18}O_3$, 378.1256; Found, 378.1256.

Synthesis of 10*H*-spiro[anthracene-9,9'-xanthen]-10-one (1c)

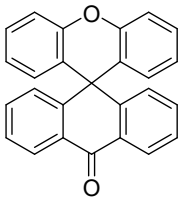

1b (1.0 g, 2.64 mmol) was dissolved in acetic acid (30 mL) and refluxed for 30 min, then concentrated HCl (2 mL) was added dropwise into the reaction solution. After the mixture was refluxed overnight, the solvent was evaporated under reduced pressure and purified by column chromatography on silica gel using dichloromethane/*n*-hexane (1:2, *v/v*) to afford **1c** as a white powder (Yield: 0.91 g, 96%). ^{1}H NMR ($CDCl_3$): δ 8.43 (dd, J = 7.7, 1.2 Hz, 2H), 7.47–7.38 (m, 4H), 7.28–7.19 (m, 4H), 7.14 (d, J = 7.5 Hz, 2H), 6.83 (td, J = 7.4, 1.2 Hz, 2H), 6.55 (dd, J = 7.9, 1.1 Hz, 2H). ^{13}C NMR (CD_2Cl_2): δ 183.8, 151.0, 149.5, 134.1, 131.8, 130.6, 129.6, 128.3, 127.1, 126.8, 126.7, 123.7, 116.9, 46.0. HRMS (EI): m/z Calcd for $C_{26}H_{16}O_2$, 360.1150; Found, 360.1147.

Synthesis of 10-(2-(phenylamino)phenyl)-10*H*-spiro[anthracene-9,9'-xanthen]-10-ol (1d)

To a solution of *tert*-butyl (2-bromophenyl)(phenyl)carbamate (1.0 g, 2.87 mmol) in dry THF (15 mL) was added dropwise *n*-BuLi (2.5 M in *n*-hexane, 1.2 mL, 3.00 mmol) at −78 °C. The reaction mixture was stirred for 1 h at −78 °C, then 10*H*-spiro [anthracene-9,9'-xanthen]-10-one (**1c**, 0.85 g, 2.33 mmol) in dry THF (15 mL) was slowly added at −78 °C. The reaction mixture was gradually allowed to warm to room temperature and stirred at 50 °C overnight. The mixture was quenched with methanol (5 mL), 1.0 M HCl

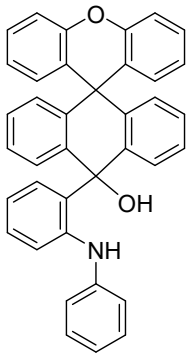

(10 mL), and water (100 mL) in order. The reaction mixture was extracted with dichloromethane and the organic layer was dried over $MgSO_4$, filtered, and evaporated under reduced pressure. The crude product was purified by column chromatography on silica gel using diethyl ether/dichloromethane (1:2, *v/v*) as eluent. The eluate was concentrated under reduced pressure and recrystallized in dichloromethane/*n*-hexane to give **1d** as a white powder (Yield: 0.89 g, 71%) ^{1}H NMR (CD_2Cl_2): δ 7.72 (t, J = 7.4 Hz, 2H), 7.65–7.58 (m, 3H), 7.54–7.51 (m, 2H), 7.35–7.19 (m, 9H), 7.14–7.11 (m, 2H), 7.08–7.04 (m, 2H), 7.00–6.91 (m, 3H), 6.71 (d, J = 7.3 Hz, 1H), 6.59 (d, J = 8.2 Hz, 1H). ^{13}C NMR (CD_2Cl_2): δ 150.1, 148.9, 148.5, 144.7, 138.5, 137.4, 134.8, 132.0, 132.0, 131.2, 130.36, 129.8, 129.4, 129.2, 129.1, 128.9, 128.6, 128.1, 127.8, 127.4, 127.2, 124.2, 123.5, 123.5, 116.7, 116.4, 115.3, 83.8, 46.2. HRMS (EI): m/z Calcd for $C_{38}H_{27}NO_2$, 529.2042; Found, 529.2040.

Synthesis of 10*H*-dispiro[acridine-9,9'-anthracene-10',9''-xanthene] (1e, O-tsACH)

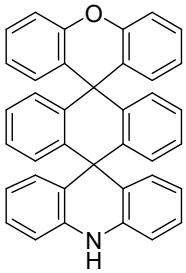

1d (0.80 g, 1.51 mmol) was dissolved in acetic acid (50 mL) and refluxed for 30 min, then concentrated HCl (2 mL) was added dropwise into the reaction solution. After the mixture was refluxed overnight, the white turbid solution was evaporated under reduced pressure and purified by column chromatography on silica gel using dichloromethane/*n*-hexane (2:3, *v/v*) to afford **1e** as a white pinky powder (Yield: 0.64 g, 83%). ^{1}H NMR (CD_2Cl_2): δ 7. ^{13}C NMR (CD_2Cl_2): δ 7.35–7.26 (m, 6H), 7.19–6.90 (m,. 14H), 6.79–6.75 (m, 4H), 6.63 (s, 1H). ^{13}C NMR (CD_2Cl_2): δ 150.1, 132.3, 130.9, 130.9, 130.9, 130.6, 129.7, 127.7, 127.21, 127.0, 123.5, 116.7, 46.7. HRMS (EI): m/z Calcd for $C_{38}H_{25}NO$, 511.1936; Found, 511.1937.

Synthesis of O-tsAC-BAsBP (1)

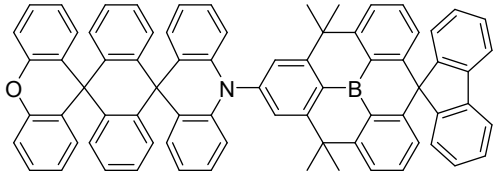

The mixture of 10*H*-dispiro[acridine-9,9'-anthracene-10',9''-xanthene] (**1e**, 0.14 g, 0.27 mmol), Br-BAsBP (0.16 g, 0.28 mmol), *t*-BuONa (0.07 g, 0.73 mmol), and Pd(*t*-$Bu_3P)_2$ (0.03 g, 0.06 mmol) in dry toluene (30 mL) were stirred at 110 °C for 2 days under a nitrogen atmosphere. After evaporating the solvent under reduced pressure, the residue was purified by column chromatography on silica gel using dichloromethane as eluent and recrystallized from a mixed solution of dichloromethane/methanol to afford **1** as a pale yellow powder (Yield: 0.20 g, 75%). ^{1}H NMR (CD_2Cl_2): δ 7.99 (d, J = 7.5 Hz, 2H), 7.93 (s, 2H), 7.71 (d, J = 7.6 Hz, 2H), 7.64 (d, J = 8.1 Hz, 2H), 7.49–7.30 (m, 8H), 7.25–7.19 (m, 6H), 7.13–6.91 (m, 12H), 6.81 (td, J = 6.9, 1.6 Hz, 2H), 6.65 (dd, J = 8.3, 0.9 Hz, 2H), 6.54 (d, J = 7.5 Hz, 2H), 1.97 (s, 12H). ^{13}C NMR spectrum could not be obtained due to poor solubility in organic solvent. HRMS (EI): m/z Calcd for $C_{75}H_{52}BNO$, 993.4154; Found,

993.4147. Anal. Calcd for $C_{75}H_{52}BNO$: C, 90.62; H, 5.27; N, 1.41%. Found: C, 90.64; H, 5.07; N, 1.33%. T_{d5} = 466 °C.

Synthesis of S-tsAC-BAsBP (2)

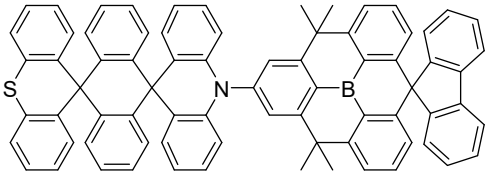

This compound was prepared in a manner analogous to the synthesis of **1** using 10*H*-dispiro[acridine-9,9'-anthracene-10',9''-thioxanthene] (**2e**, 0.15 g, 0.28 mmol), Br-BAsBP (0.16 g, 0.28 mmol), *t*-BuONa (0.07 g, 0.73 mmol), and Pd(*t*-$Bu_3P)_2$ (0.02 g, 0.04 mmol) in dry toluene (30 mL) to give **2** as a pale yellow powder (Yield: 0.26 g, 89%). ^{1}H NMR (CD_2Cl_2): δ 7.99 (d, J = 7.6 Hz, 2H), 7.94 (s, 2H), 7.70 (t, J = 7.5 Hz, 4H), 7.52–7.39 (m, 8H), 7.23 (td, J = 7.1, 1.5 Hz, 6H), 7.14–6.98 (m, 8H), 6.92 (td, J = 7.5, 1.5 Hz, 4H), 6.80 (td, J = 7.2, 1.2 Hz, 2H), 6.67 (dd, J = 8.4, 0.9 Hz, 2H), 6.54 (d, J = 7.5 Hz, 2H), 1.97 (s, 12H). ^{13}C NMR spectrum could not be obtained due to poor solubility in organic solvent. HRMS (EI): m/z Calcd for $C_{75}H_{52}BNS$, 1009.3926; Found, 1009.3910. Anal. Calcd for $C_{75}H_{52}BNS$: C, 89.18; H, 5.19; N, 1.39%. Found: C, 88.86; H, 4.83; N, 1.29%. T_{d5} = 464 °C.

Cyclic Voltammetry

Cyclic voltammetry measurements for oxidation were carried out in dichloromethane (1.0×10^{-4} M) using a three-electrode cell configuration comprising platinum working and counter electrodes and an $Ag/AgNO_3$ (0.01 M in CH_3CN) reference electrode at room temperature. Tetra-*n*-butylammonium hexafluorophosphate (0.1 M) was used as the supporting electrolyte. The oxidation potentials were recorded at a scan rate of 100 mV s^{-1} and were reported with reference to the ferrocene/ferrocenium (Fc/Fc^+) redox couple. The HOMO energy levels were determined from the onset value of electrochemical oxidation of cyclic voltammograms while the LUMO energy levels were estimated from the optical bandgap (E_g) and the HOMO levels.

Photophysical Measurements

The UV/Vis absorption and photoluminescence (PL) spectra were recorded on a Varian Cary 100 and an FLS1000 (Edinburgh Instruments) spectrophotometer, respectively. Solution PL spectra were obtained from oxygen-free and air-saturated solutions. Photoluminescence quantum yields (PLQYs) of the samples were measured on an absolute PL quantum yield spectrophotometer (Quantaurus-QY C11347-11, Hamamatsu Photonics). Transient PL decays were measured on an FLS1000 spectrophotometer in time-correlated single-photon counting (TCSPC) mode using an EPL-375 picosecond pulsed diode laser as an excitation source. PLQYs of prompt (Φ_p) and delayed (Φ_d) fluorescence were estimated from the prompt

and delayed components of the transient decay curves, respectively. The temperature-dependence of PL decay was obtained with an OptistatDN^{TM} cryostat (Oxford Instruments). Rate constants of fluorescence radiative decay, $k_r = \Phi_p/\tau_p$, intersystem crossing, $k_{ISC} = (1 - \Phi_p)/\tau_p$, and reverse intersystem crossing, $k_{RISC} = (k_p k_d \Phi_d)/(k_{ISC} \Phi_p) = \Phi_d/(k_{ISC} \tau_p \tau_d \Phi_p)$, where Φ_p and Φ_d are the quantum yields for prompt and delayed fluorescence ($\Phi_{PL} = \Phi_p + \Phi_d$), respectively, were estimated from the reported method.[5] The photophysical analysis done by using FLS1000 and Quantaurus-QY C11347-11 spectrophotometers was conducted at total-period analysis center for Ulsan chemical industry of KBSI.

Theoretical Calculations

The computational study based on time-dependent density functional theory (TDDFT) was performed to investigate not only the geometric and electronic structures of ground and exited states of two D–A compounds (**1** and **2**) but also their transition properties for the reverse intersystem crossing (RISC) processes. The TDDFT calculations were carried out with Tamm-Dancoff approximation (TDA).[6] which was reported to be suitable for exmaining the lowest singlet–triplet energy gap (ΔE_{ST}), one of key peroperties in TADF process.[7] Their ground (S_0) states of compounds were optimized using DFT calculations, and their lowest singlet (S_1) and two triplet (T_1 and T_2) excited states were optimized using TDDFT calculations with the PBE0 hybrid functional[8] and 6-31+G(d,p) basis set implemented in GAUSSIAN 16 software package.[9] Natural transition orbital (NTO) analysis was performed to characterize the excited states, i.e., charge transfer (CT) and local excitation (LE).[10] The overlap integral extents between frontier molecular orbitals, HOMO and LUMO, and between hole and electron NTOs were computed using Multiwfn program.[11] The transition characteristics of the pristine donor (X-tsACH, X = O, S) and acceptor (HBAsBP) molecules were also elucidated using NTO analysis in order to rationalize the electronic structures of excited states of compounds **1** and **2** constructed in combination of donor and acceptor moieties. The non-radiative decay rate for RISC processes, i.e., $S_1 \leftarrow T_n$ (n = 1 and 2), were evaluated via thermal vibrational correlation function (TVCF) approach in Molecular Materials Property Prediction Package (MOMAP 2020B).[12] The TVCF formalism is derived from Fermi's golden rule and second-order perturbation combining both non-adiabatic coupling and spin-orbit coupling, in which the mode-mixing (Duschinsky rotation effect) and the coordinate-dependent transition dipole (Herzberg-Teller effect) are accounted. Spin-orbit coupling matrix elements (SOCME) between excited S_1 and T_n (n = 1 and 2) were computed by using the quasi-degenerate perturbation theory[13] as implemented in ORCA software package[14], in which the PBE0 hybrid functional and 6-311G(d,p) basis set were used. Computationally obtained numerical data for the RISC processes are presented in **Table 2** in the main text.

Fabrication of Electroluminescent Devices

OLED devices were fabricated on 25 mm × 25 mm glass substrate with patterned ITO layers (AMG, Korea). Glass substrate with pre-patterned ITO electrodes were cleaned by a sequential wet-cleaning process in an ultrasonic bath. Then, the substrates were treated by 70W UV-plasma for 1 min in a plasma cleaner (CUTE-MP, Femto Science) as reported previously.[15] All vacuum evaporation was performed under 7.0×10^{-7} torr, and evaporation rate of organics was around 1.0 Å/s. The deposition rate was 0.2~0.3 Å/s for LiF and 1.5 Å/s for Al. The sizes of the individual pixels were 4.0 mm^2. The current density–voltage–luminance (*J–V–L*) and angle-resolved electroluminescence (EL) intensity characteristics of the fabricated devices were obtained with a source-measure unit (Keithley 2400) using a calibrated photodiode (FDS100, Thorlab) and a fiber optic spectrometer (BW_UVNb, StellarNet) held on a motorized goniometer (PRM1/MZ8, Thorlabs) in a nitrogen (N_2)-filled glove box. The EQE (η_{EQE}) and PCE (η_{PCE}) of the devices were estimated from the measured full angular characteristics without Lambertian simplification.

Optical Simulation and Analysis

Trans-scale optical simulation was realized by custom-made MATLAB codes describing coherent dipole radiation theory also termed as a "power-dissipation model" for OLED stacks. This takes into account Purcell effect, dipole orientation, and coupling to waveguide and SPP modes. The results exhibited a quantitative match with experimental data in angle-resolved and spectrally resolved manners. In the coherent optical simulation for an OLED stack, the emission zone was assumed to be located at the center of its emitting layer. Anisotropy was also considered and the electrical loss was assumed to be absent.

Angle-dependent PL Intensity Measurements

Emission layer was deposited on the bare glass substrate with 50 nm-thick. Then, glass encapsulation was done in nitogen (N_2)-filled glove box. Full angular *p*-polarized PL measurements were carried out with the goniometer based motorized intensity measurement system (Phelos by Fluxim AG, Switzerland). Simulation and fitting with the experimental data were made with a customized MATLAB code describing coherent dipole radiation theory described above.

Horizontal orientation of transition dipole moment

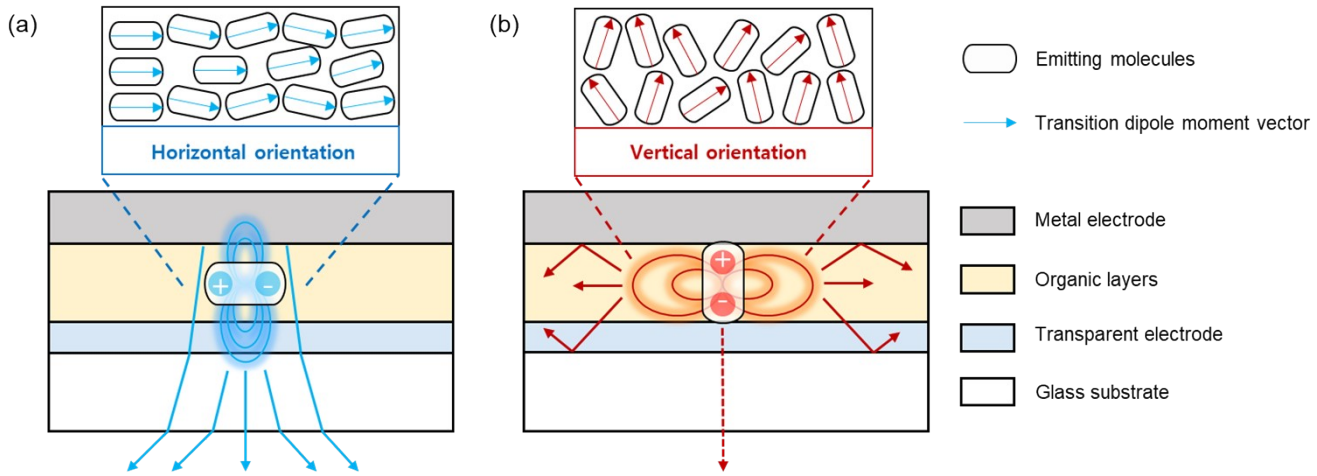

Fig. S1. The schematic image shows how the horizontal orientation of the transition dipole moment of emitting molecules contributes to the enhancement of the outcoupling efficiency in OLEDs. As light propagates perpendicularly to the oscillation of the emitting dipole, an emission layer having high $\Theta_{//}$ emits a larger number of photons externally (a) compared to those based on emission layers with predominantly vertical orientation (b). $\Theta_{//}$ of an emission layer composed of a given molecule is larger than 67%.

NMR Spectra

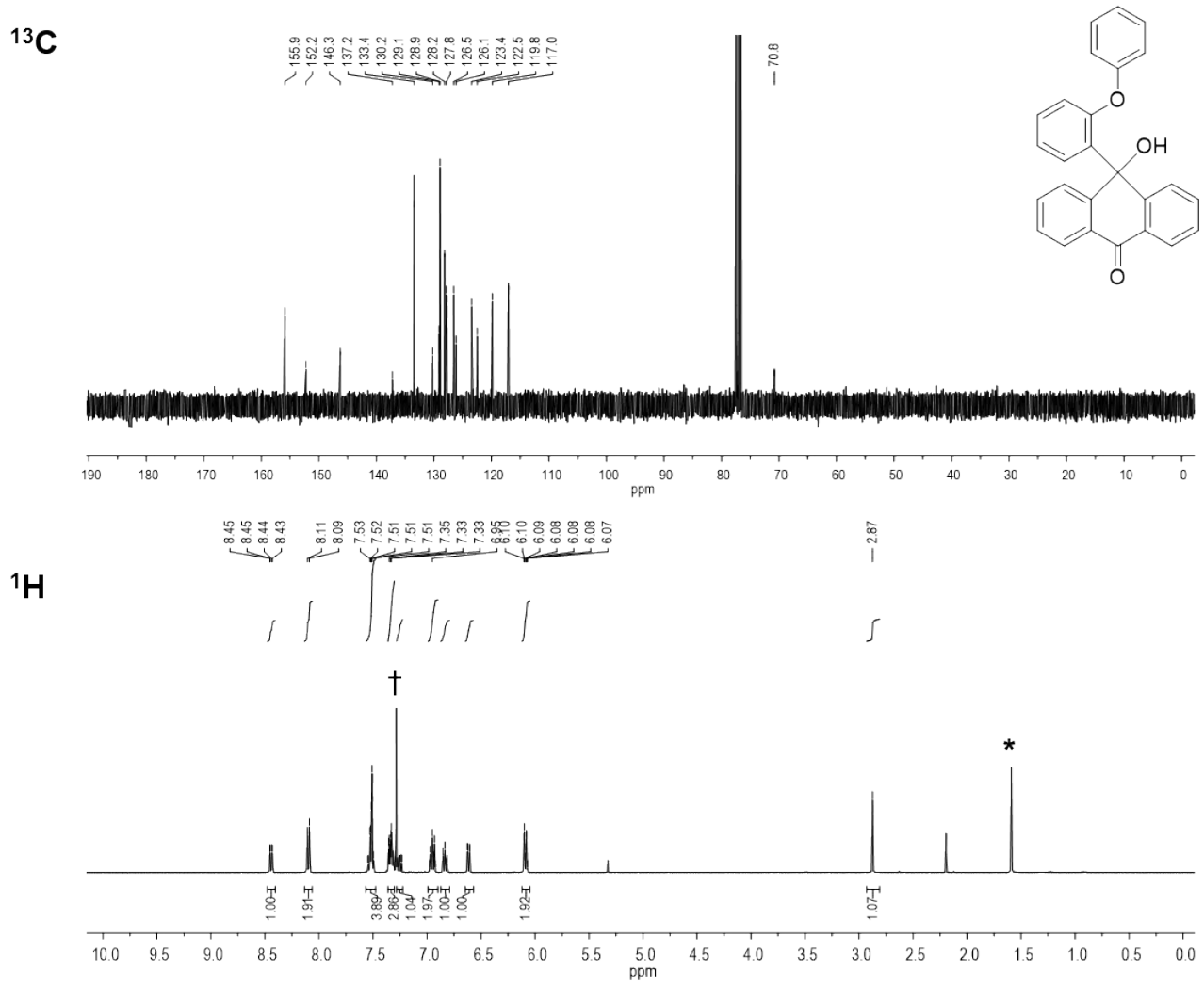

Fig. S2. NMR spectra of **1b** in $CDCl_3$ (∗ from water and † from residual $CHCl_3$).

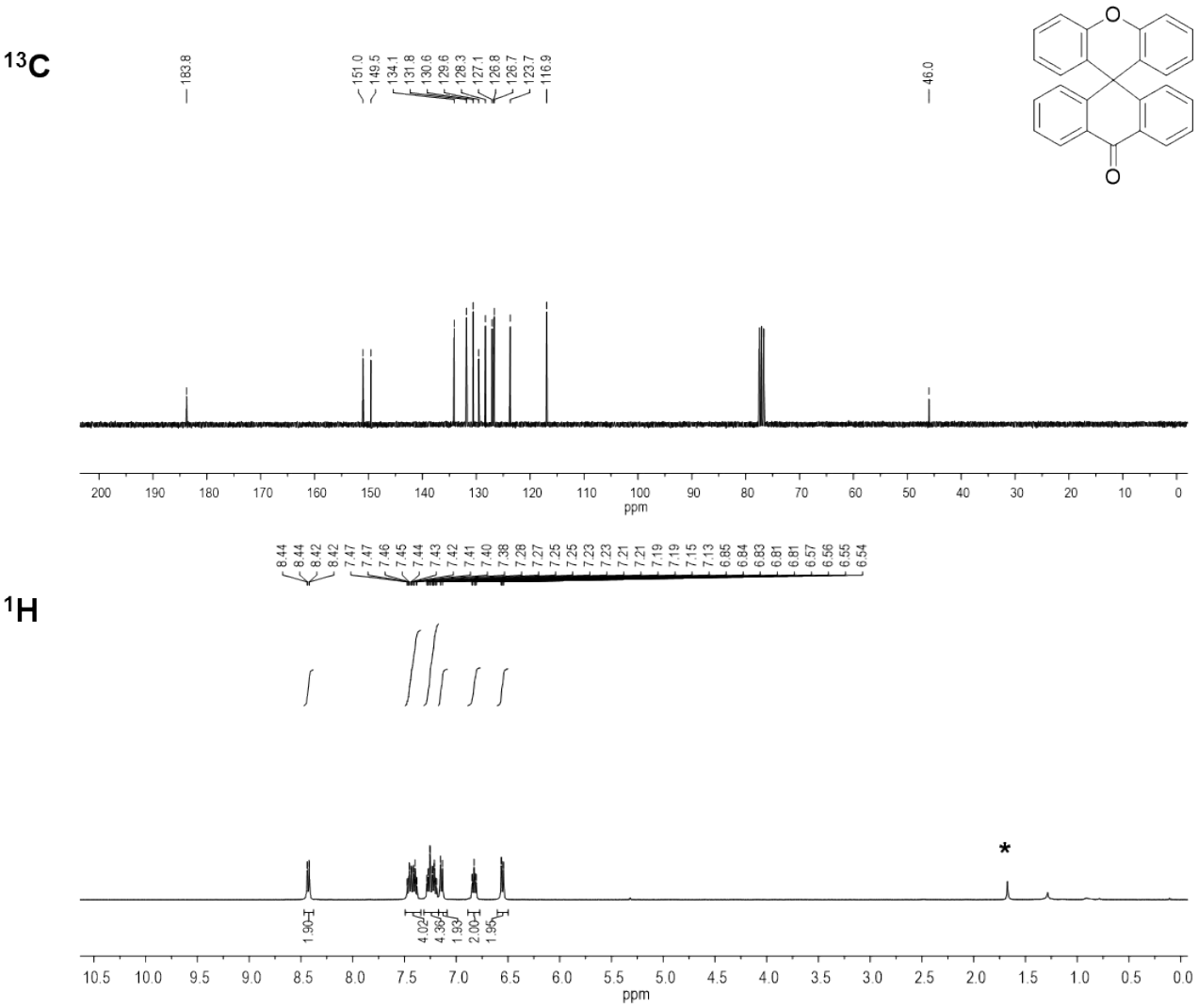

Fig. S3. NMR spectra of **1c** in $CDCl_3$ (∗ from water).

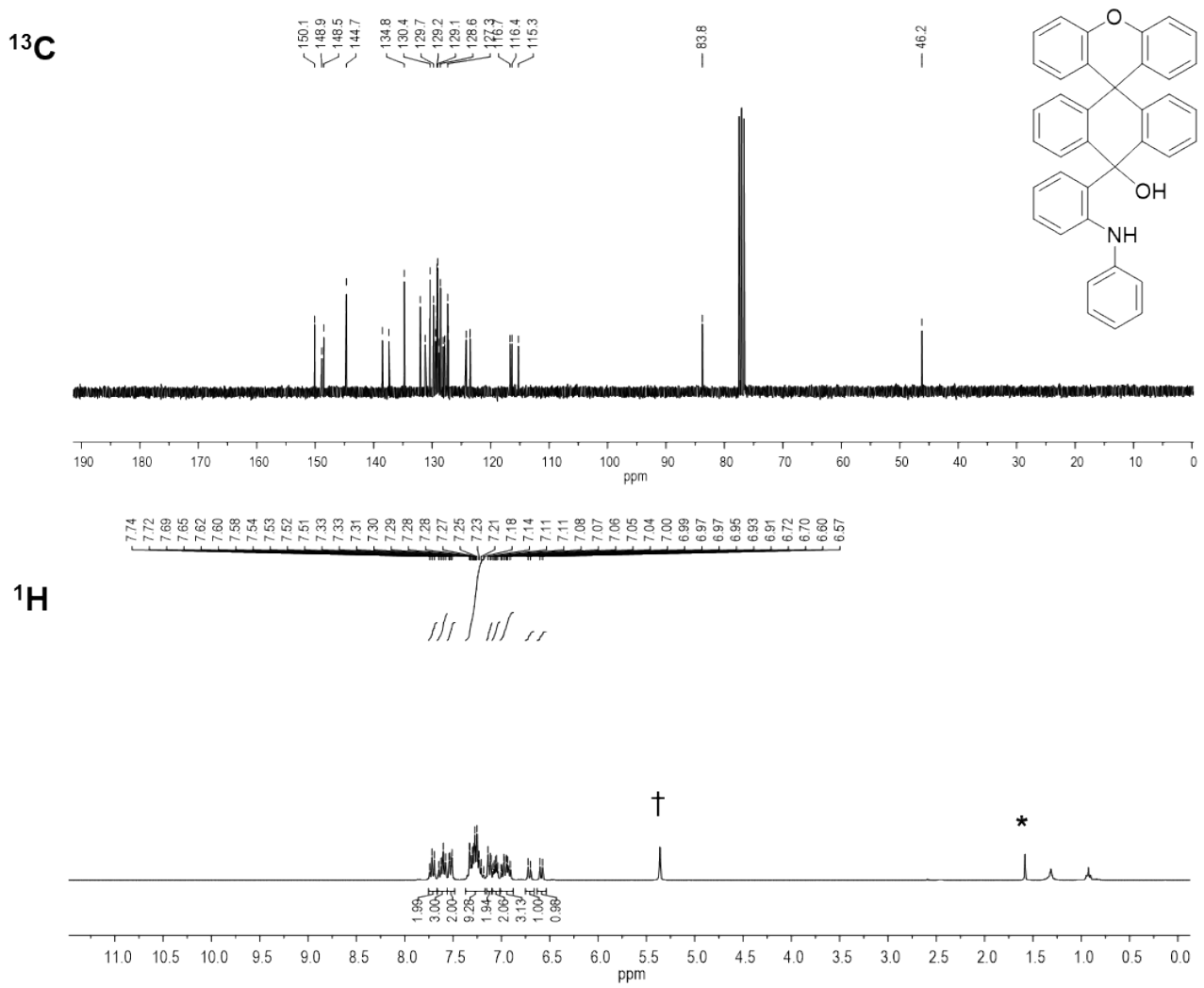

Fig. S4. NMR spectra of **1d** in CD_2Cl_2 (∗ from water and † from residual $CHDCl_2$).

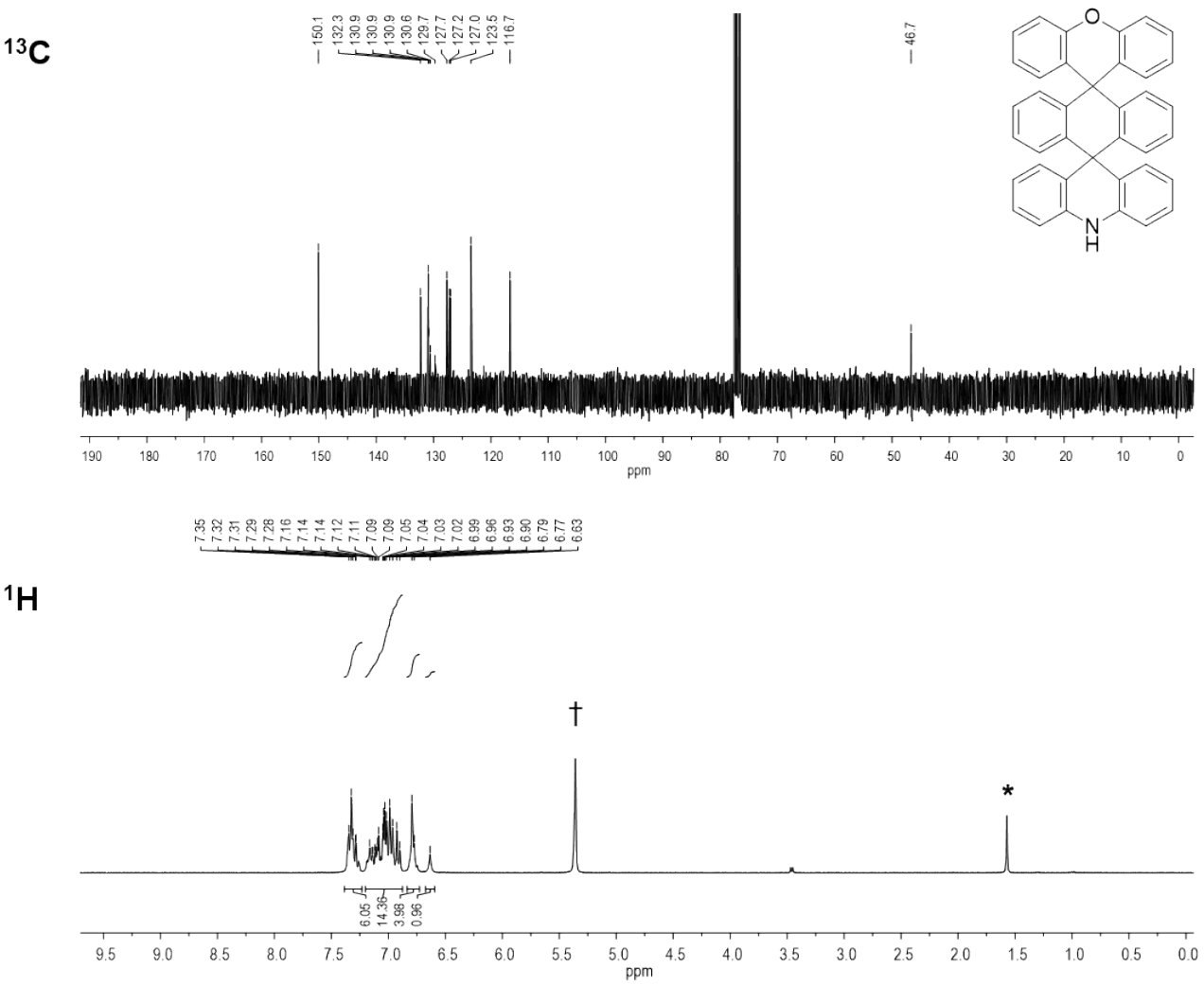

Fig. S5. NMR spectra of **1e** (O-tsACH) in CD_2Cl_2 (∗ from water and † from residual $CHDCl_2$).

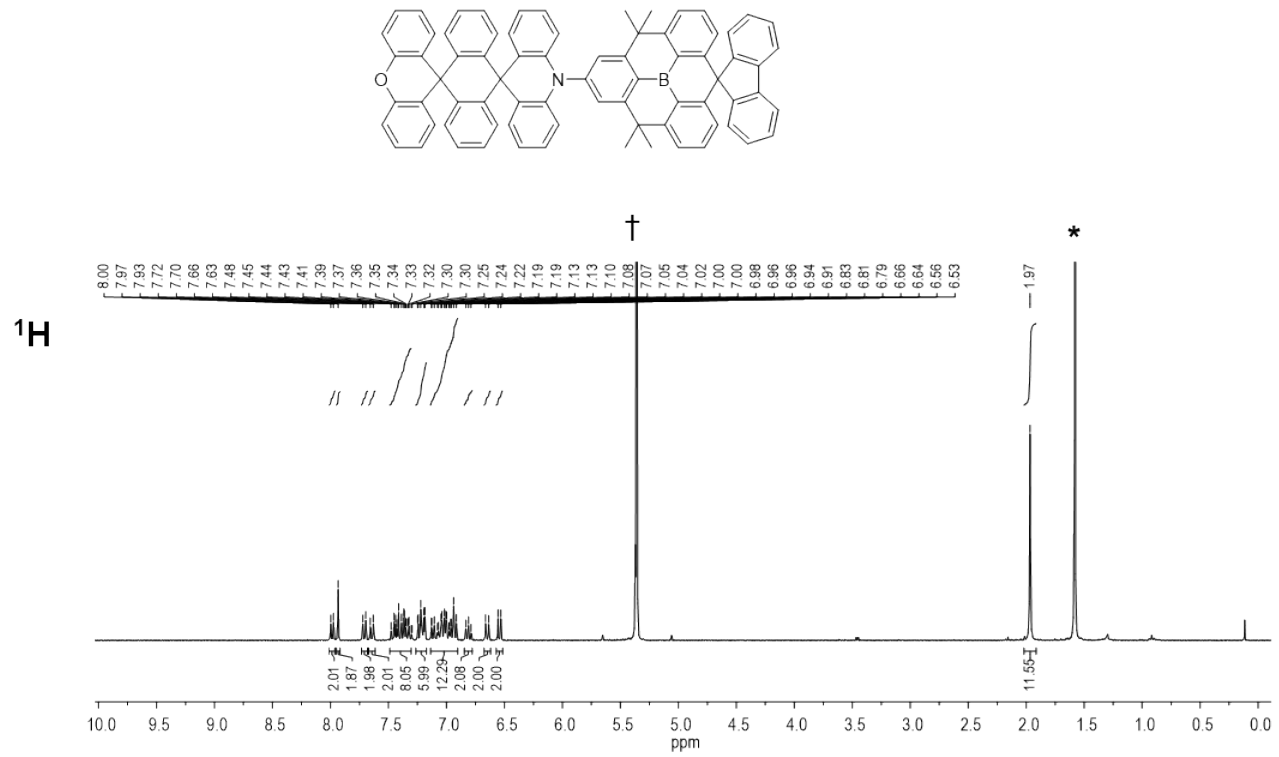

Fig. S6. NMR spectra of O-tsAC-BAsBP (**1**) in CD_2Cl_2 (∗ from water and † from residual $CHDCl_2$).

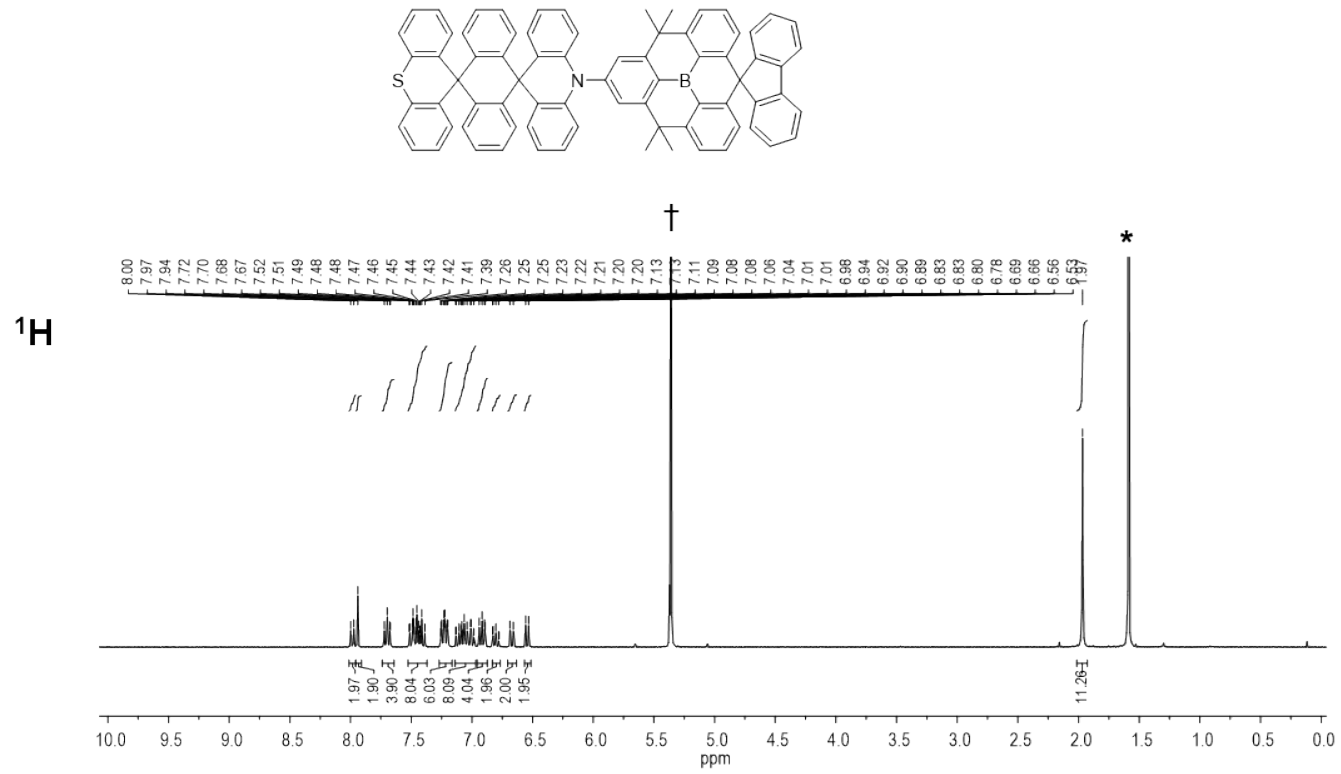

Fig. S7. NMR spectra of S-tsAC-BAsBP (**2**) in CD_2Cl_2 (∗ from water and † from residual $CHDCl_2$).

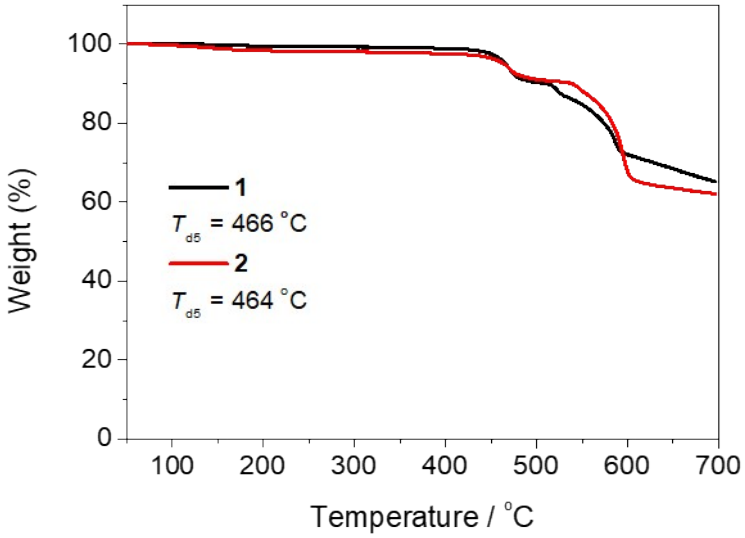

Fig. S8. TGA curves of **1** and **2**.

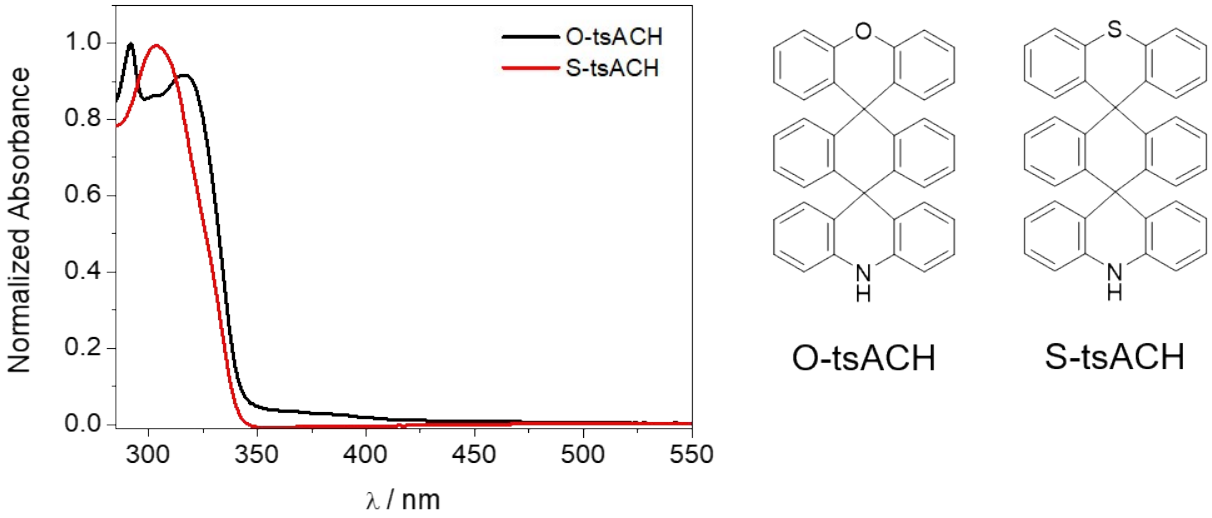

Fig. S9. UV/Vis absorption spectra of the pristine donor molecules in toluene.

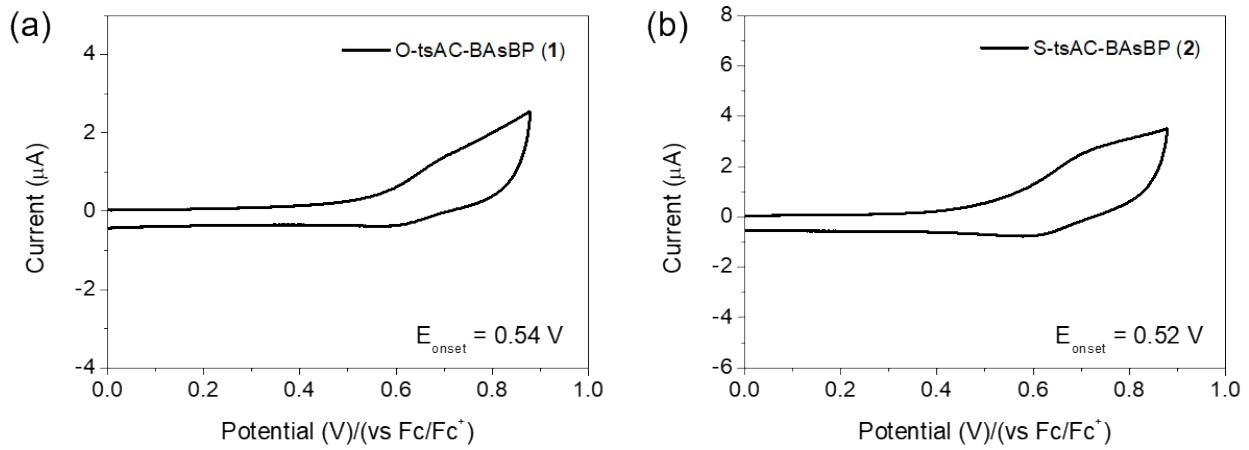

	E_g (eV)[a]	E_{oxd} (V)[b]	E_{HOMO} (eV)	E_{LUMO} (eV)
O-tsAC-BAsBP (**1**)	2.93	0.54	−5.34	−2.41
S-tsAC-BAsBP (**2**)	2.93	0.52	−5.32	−2.39

[a] E_g: optical bandgap from the absorption onset wavelength. [b] E_{oxd}: oxidation onset potential.

Fig. S10. Cyclic voltammograms of (a) **1** and (b) **2** showing oxidation (1.0×10^{-4} M in CH_2Cl_2, scan rate = 100 mV/s).

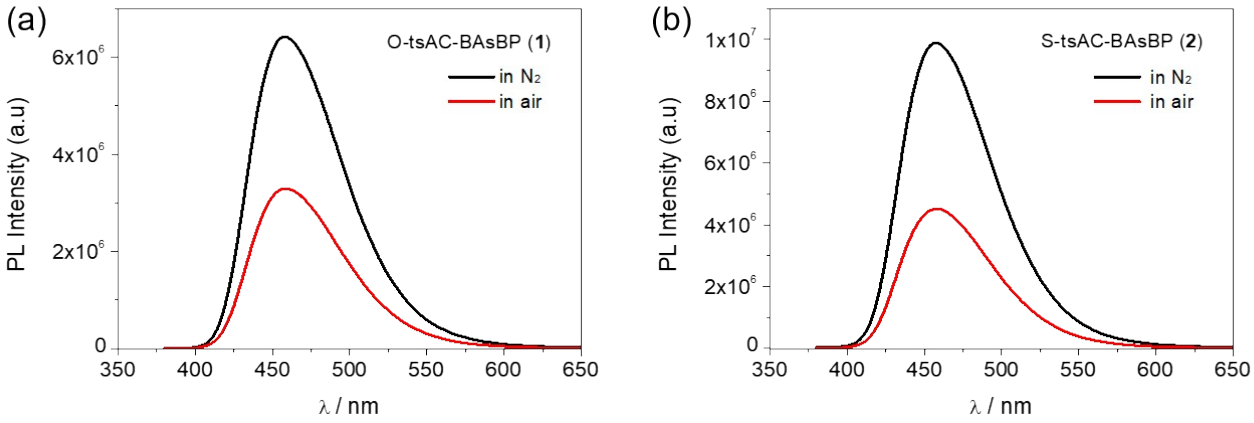

Fig. S11. PL spectra of (a) **1** and (b) **2** in oxygen-free (black line) and air-saturated (red line) toluene at 298 K.

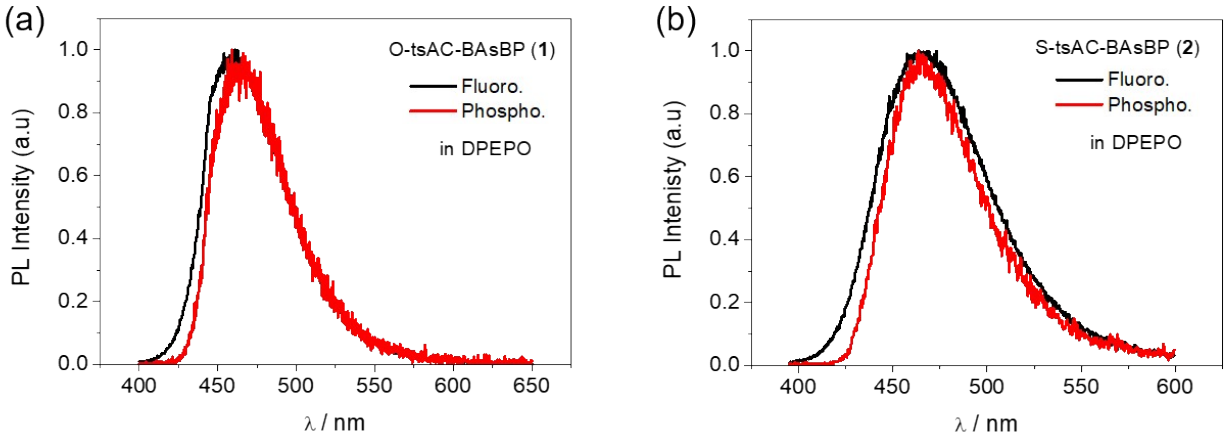

Fig. S12. Fluorescence and phosphorescence spectra of the DPEPO host films doped with 20 wt% of (a) **1** and (b) **2** at 77 K.

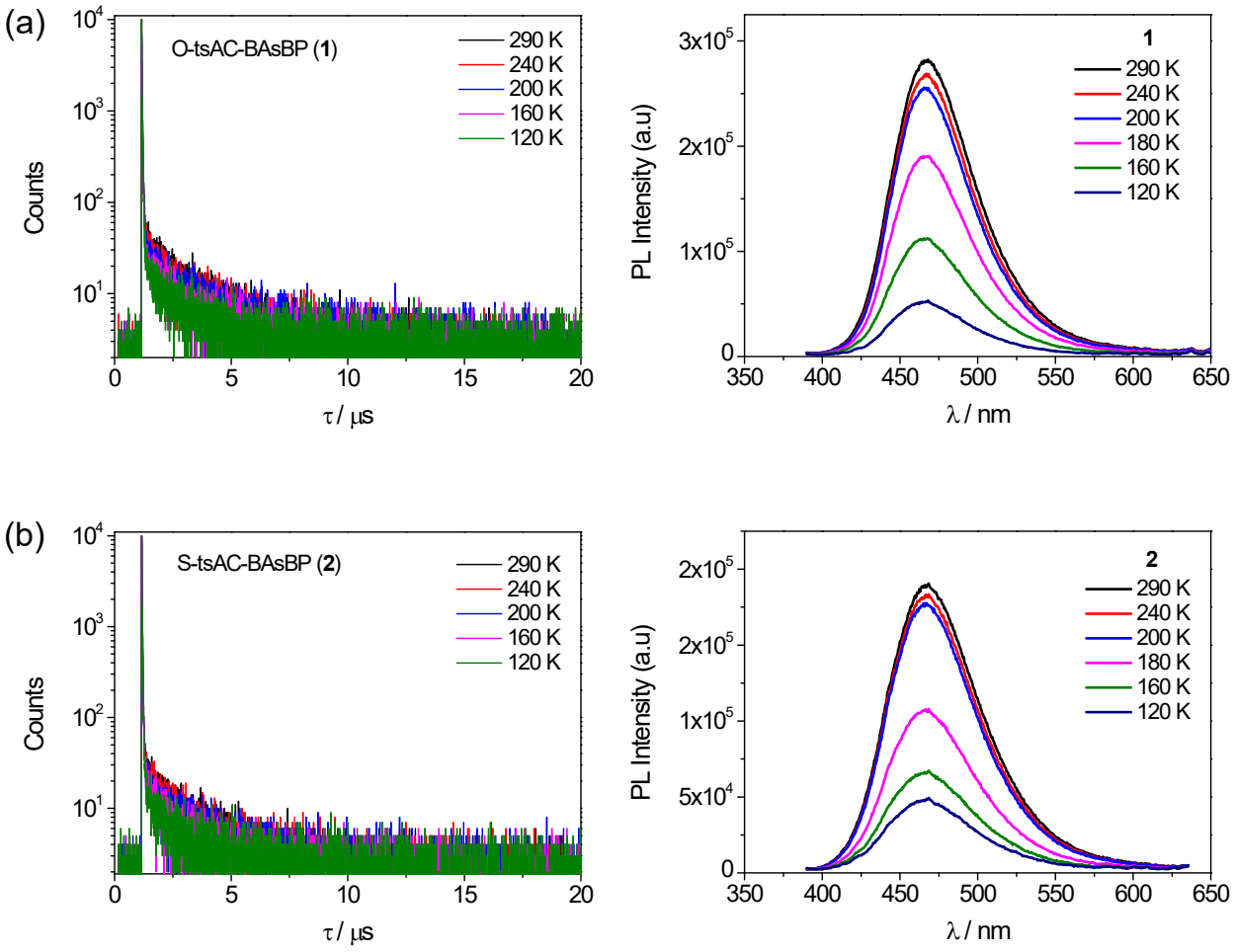

Fig. S13. Transient PL decay curves (left) and PL spectra (right) of the DPEPO host films doped with 20 wt% of (a) **1** and (b) **2** at various temperatures.

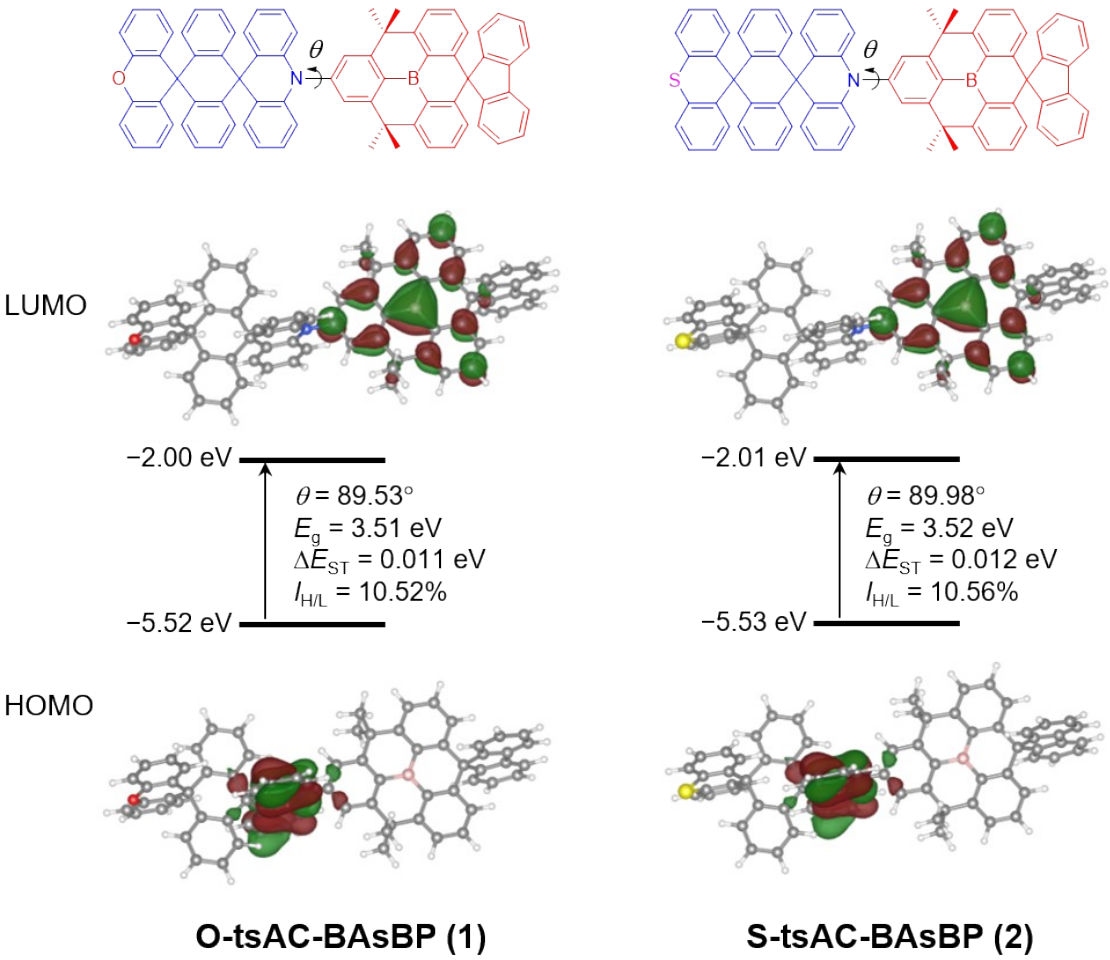

Fig. S14. Frontier molecular orbitals of **1** and **2** (isovalue = 0.03 e/Å^3) at their ground state (S_0) geometries obtained using PBE0/6-31+G(d,p) calculations. The numerical values for MO energies, dihedral angles (θ), HOMO–LUMO gaps (E_g), S_1–T_1 energy splitting (ΔE_{ST}), and overlap integrals ($I_{H/L}$) between HOMO and LUMO are provided.

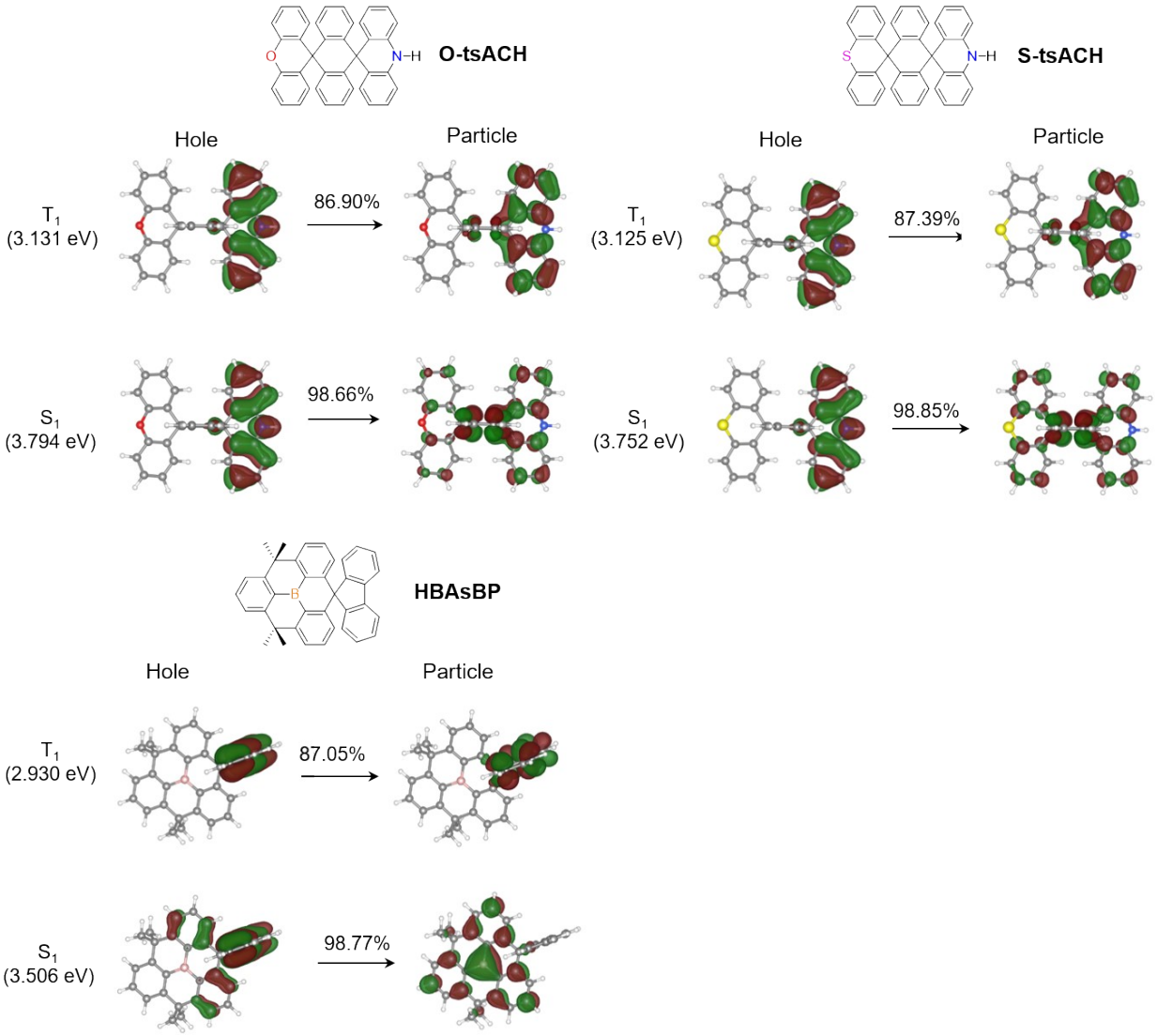

Fig. S15. Natural transition orbitals (NTOs) of the pristine donor (X-tsACH, X = O, S) and acceptor (HBAsBP) molecules in **1** and **2** for the transitions from S_0 to S_1 and T_1 states obtained using the TDDFT calculations at the PBE0/6-31+g(d,p) level of theory. The adiabatic excitation energies are given in parentheses.

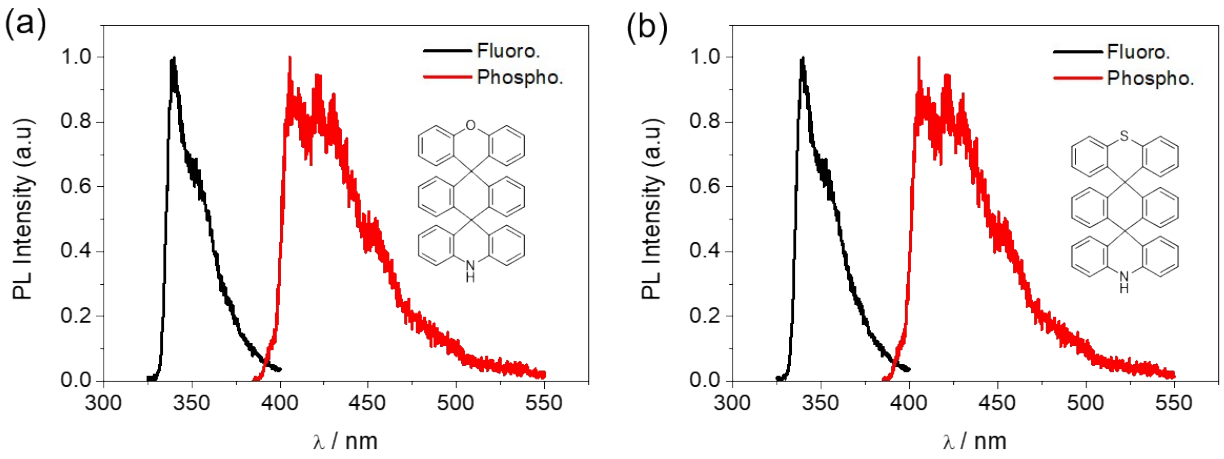

Fig. S16. Fluorescence (blak line) and phosphorescence (red line) spectra of (a) O-tsACH and (b) S-tsACH in toluene at 77 K.

Table S1. Photophysical data and rate constants of **1** and **2** doped in a DPEPO host.

Compd	Conc. (wt%)	λ_{PL} (nm)	Φ_{PL}[a] (%)	$\Theta_{//}$[b] (%)	τ_p[c] (ns)	τ_d[c] (μs)	E_S/E_T[d] (eV)	ΔE_{ST}[e] (meV)	k_r[f] (10^7 s^{-1})	k_{ISC}[f] (10^7 s^{-1})	k_{RISC}[f] (10^5 s^{-1})	E_a^{RISC}[g] (meV)
O-tsAC-BAsBP (**1**)	20	467	100	93.0	16	1.55	2.89/2.86	15	4.06	2.23	9.99	15
	10	458	82		13	1.81						
S-tsAC-BAsBP (**2**)	20	469	84	93.5	14	1.98	2.95/2.90	13	4.68	1.57	6.86	13
	10	462	100		16	1.71						

[a] Absolute PLQYs.

[b] Horizontal dipole orientation ratio.

[c] Prompt (τ_p) and delayed (τ_d) PL decay lifetimes.

[d] Singlet (E_S) and triplet (E_T) energy deduced from the onset of fluorescence and phosphorescence spectra at 77 K.

[e] $\Delta E_{ST} = E_S - E_T$.

[f] k_r, k_{ISC}, and k_{RISC} are the rate constants of fluorescence radiative decay, intersystem crossing, and reverse intersystem crossing (RISC), respectively.

[g] Activation energies of RISC.

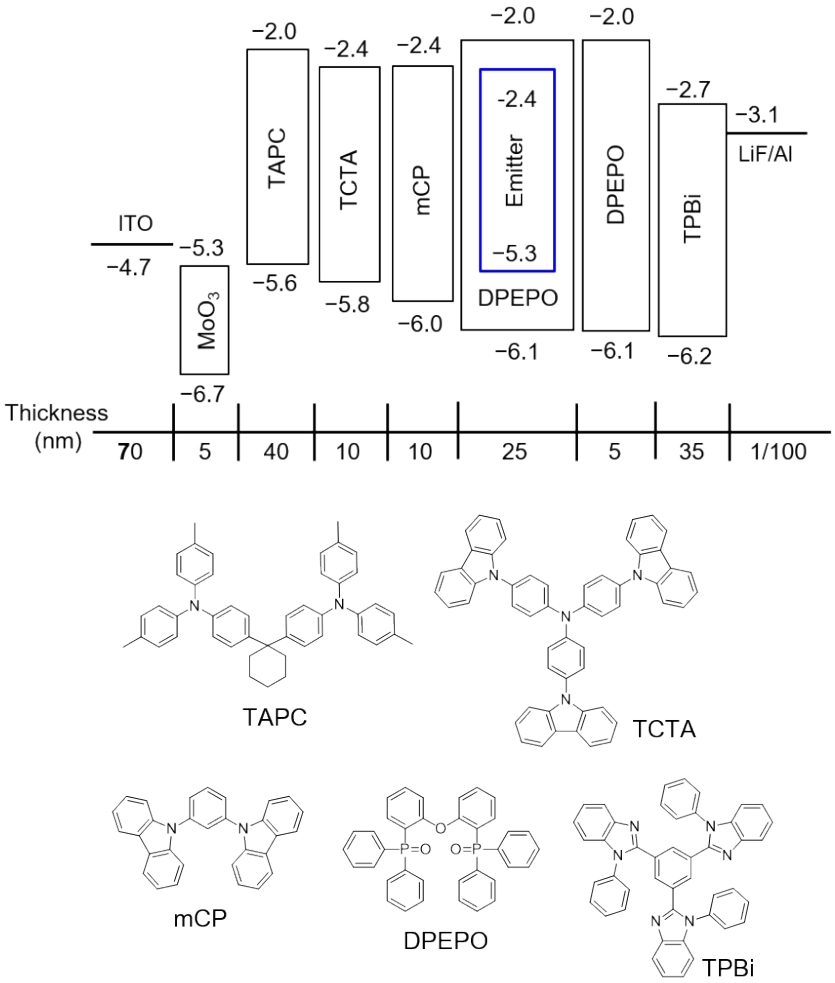

Fig. S17. (Top) Device structure and energy level diagram (in eV) of the TADF-OLEDs relative to the vacuum level and (bottom) chemical structures of the consisting layers.

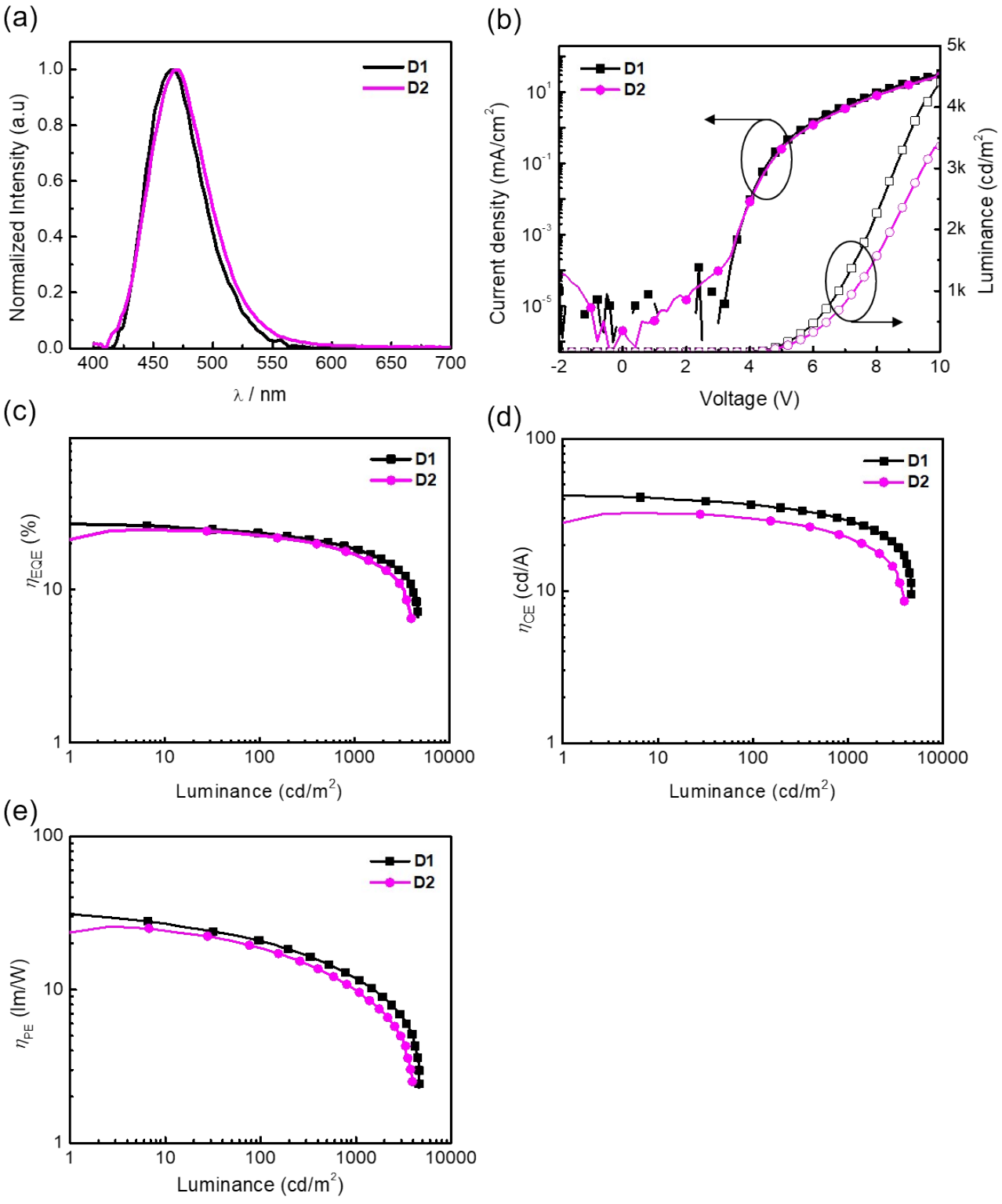

Fig. S18. (a) EL spectra, (b) Current density–voltage–luminance (*J*–*V*–*L*) characteristics, (c) External quantum efficiency–luminance (η_{EQE}–*L*) characteristics, (d) Current efficiency–luminance (η_{CE}–*L*) characteristics, and (e) power efficiency–luminance (η_{PE}–*L*) characteristics of **D1** and **D2**.

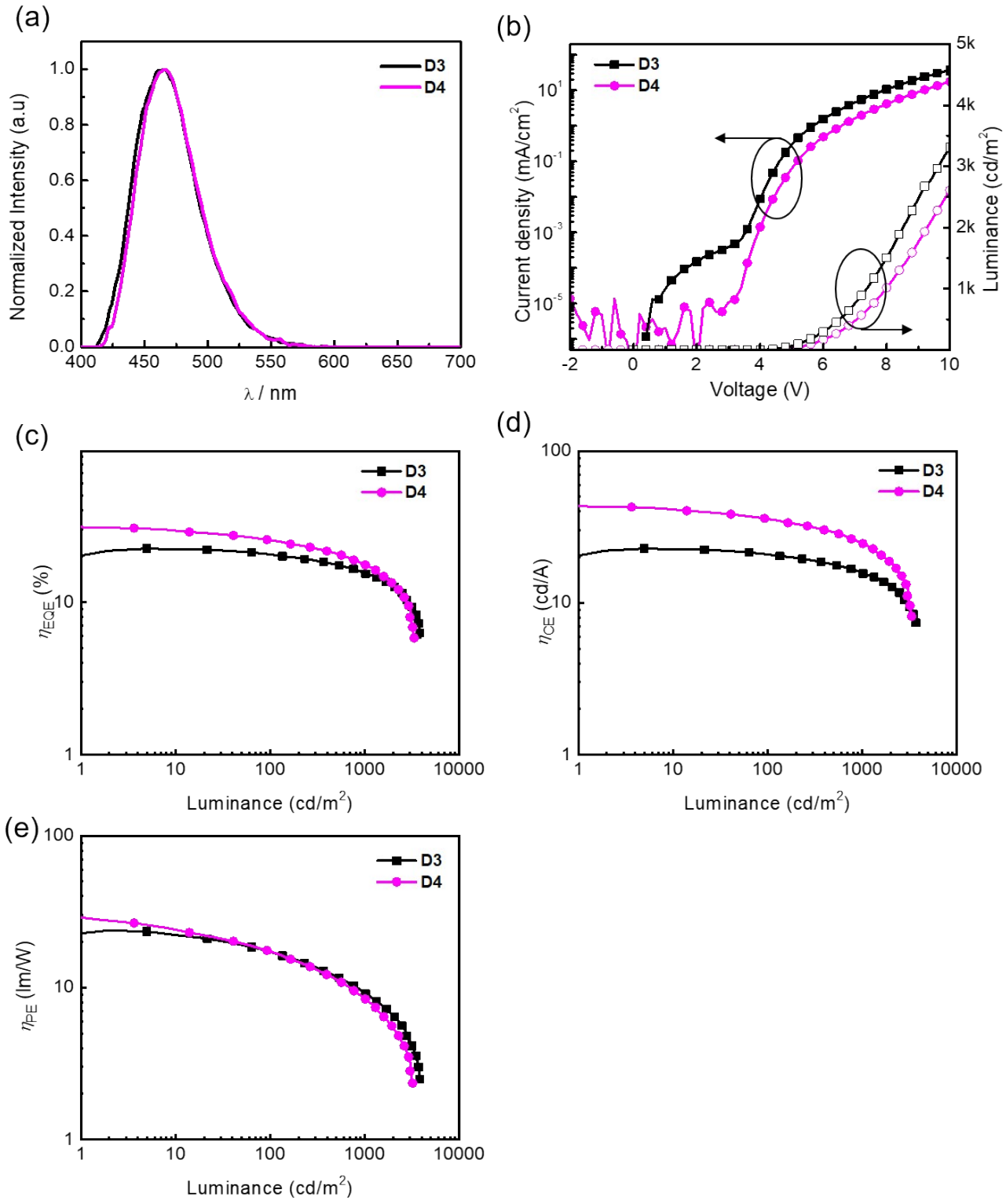

Fig. S19. (a) EL spectra, (b) Current density–voltage–luminance (*J*–*V*–*L*) characteristics, (c) External quantum efficiency–luminance (η_{EQE}–*L*) characteristics, (d) Current efficiency–luminance (η_{CE}–*L*) characteristics, and (e) power efficiency–luminance (η_{PE}–*L*) characteristics of **D3** and **D4**.

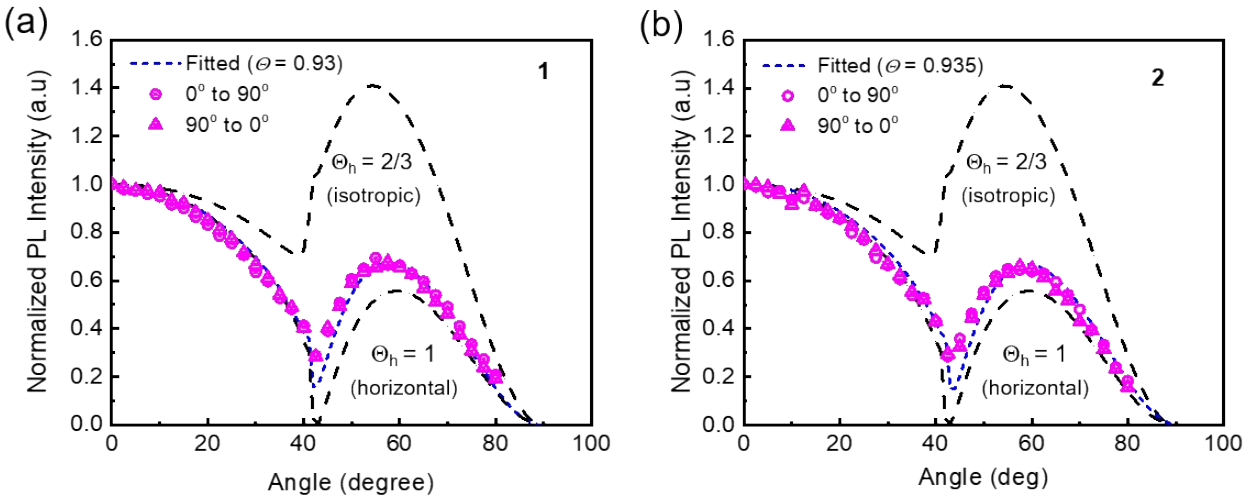

Fig. S20. Angle-dependent PL intensity of the emitting layer of (a) **1** and (b) **2**. The circyle symbols are the experimental results, and the blue lines indicate the simulation data to determine the horizontal dipole ratios of the emitters.

References

1. A. Kumar, B. S. Bhakuni, Ch. D. Prasad, S. Kumar and S. Kumar, Potassium *tert*-Butoxide-Mediated Synthesis of Unsymmetrical Diaryl Ethers, Sulfides and Selenides from Aryl Bromides. *Tetrahedron* **2013**, *69*, 5383–5392.

2. L. Wang, X. Cai, B. Li, M. Li, Z. Wang, L. Gan, Z. Qiao, W. Xie, Q. L., N. Zheng, K. Liu and S.-J. Su, Achieving nhanced Thermally Activated Delayed Fluorescence Rates and Shortened Exciton Lifetimes by Constructing Intramolecular Hydrogen Bonding Channels. *ACS Appl. Mater. Interfaces*, **2019**, *11*, 45999−46007.

3. W. Li, B. Li, X. Cai, L. Gan, Z. Xu, W. Li, K. Liu, D. Chen and S.-J. Su, Tri-Spiral Donor for High Efficiency and Versatile Blue Thermally Activated Delayed Fluorescence Materials. *Angew. Chem. Int. Ed*. **2019**, *58*, 11301–11305.

4. Y. H. Lee , W. Lee, T. Lee, J. Jung, S. Yoo and M. H. Lee, Achieving over 36% EQE in Blue OLEDs Using Rigid TADF Emitters Based on Spiro-Donor and Spiro-*B*-Heterotriangulene Acceptors. *Chem. Eng. J*. **2023**, *452*, 139387.

5. K.-C. Pan, S.-W. Li , Y.-Y. Ho, Y.-J. Shiu, W.-L. Tsai, M. Jiao, Wei-K. Lee, Ch.-C. Wu, C.-L. Chung, T. Chatterjee, Y.-S. Li, K.-T. Wong, H.-C. Hu, C.-C. Chen and M.-T. Lee, Efficient and Tunable Thermally Activated Delayed Fluorescence Emitters Having Orientation-Adjustable CN-Substituted Pyridine and Pyrimidine Acceptor Units. *Adv. Funct. Mater*. **2016**, *26*, 7560−7571.

6. S. Hirata and M. Head-Gordon, Time-Dependent Density Functional Theory within the Tamm–Dancoff Approximation**.** *Chem. Phys. Lett.* **1999**, *314*, 291–299.

7. M. Moral, L. Muccioli, W.-J. Son, Y. Olivier and J. C. Sancho-García, Theoretical Rationalization of the Singlet−Triplet Gap in OLEDs Materials: Impact of Charge-Transfer Character. *J. Chem. Theory Comput.* **2015**, *11*, 168−177.

8. C. Adamo and V. Barone, Toward Reliable Density Functional Methods without Adjustable Parameters: The PBE0 Model. *J. Chem. Phys.* **1999**, *110*, 6158−6169.

9. M. J. Frisch, G. W. Trucks, H. B. Schlegel, G. E. Scuseria, M. A. Robb, J. R. Cheeseman, G. Scalmani, V. Barone, G. A. Petersson, H. Nakatsuji, X. Li, M. Caricato, A. V. Marenich, J. Bloino, B. G. Janesko, R. Gomperts, B. Mennucci, H. P. Hratchian, J. V. Ortiz, A. F Izmaylov, J. L. Sonnenberg. D. Williams-Young, F. Ding, F. Lipparini, F. Egidi, J. Goings, B. Peng, A. Petrone, T. Henderson, D. Ranasinghe, V. G. Zakrzewski, J. Gao, N. Rega, G. Zheng, W. Liang, M. Hada, M. Ehara, K. Toyota, R. Fukuda, J. Hasegawa, M. Ishida, T. Nakajima, Y. Honda, O. Kitao, H. Nakai, T. Vreven, K. Throssell, J. A. Jr. Montgomery, J. E. Peralta, F. Ogliaro, M. J. Bearpark, J. J. Heyd, E. N. Brothers, K. N. Kudin, V. N. Staroverov, T. A. Keith, R. Kobayashi, J. Normand, K. Raghavachari, A. P. Rendell, J. C. Burant, S. S. Iyengar, J. Tomasi, M. Cossi, J. M. Millam, M. Klene, C. Adamo, R. Cammi, J. W. Ochterski, R. L. Martin, K. Morokuma, O. Farkas, J. B. Foresman and D. J. Fox, Gaussian 16, Revision A.03, Gaussian, Inc., Wallingford CT, **2016**.

10. R. L. Martin, Natural Transition Orbitals. *J. Chem. Phys.* **2003**, *118*, 4775–4777.

11. T. Lu and F. Chen, Multiwfn: A Multifunctional Wavefunction Analyzer. *J. Comput. Chem*. **2012**, *33*, 580–592.

12. (a) Z. Shuai, Thermal Vibration Correlation Function Formalism for Molecular Excited State Decay Rates. *Chin. J. Chem.* **2020**, *38*, 1223–1232. (b) Z. Shuai and Q. Peng, Excited States Structure and Processes: Understanding Organic Light-Emitting Diodes at the Molecular Level. *Phys. Rep.* **2014**, *537*, 123–156.

13. B. de Souza, G. Farias, F. Neese and R. Izsák, Predicting Phosphorescence Rates of Light Organic Molecules Using Time-Dependent Density Functional Theory and the Path Integral Approach to Dynamics. *Chem. Theory Comput.* **2019**, *15*, 1896-1904.
14. F. Neese, F. Wennmohs, U. Becker and C. Riplinger, The ORCA Quantum Chemistry Program Package. *J. Chem. Phys.* **2020**, *152*, 224108.
15. Y. H. Lee, S. Park, J. Oh, S.-J. Woo, A. Kumar, J.-J. Kim, J. Jung, S. Yoo and M. H. Lee, High-Efficiency Sky Blue to Ultradeep Blue Thermally Activated Delayed Fluorescent Diodes Based on *Ortho*-Carbazole-Appended Triarylboron Emitters: Above 32% External Quantum Efficiency in Blue Devices. *Adv. Opt. Mater.* **2018**, *6*, 1800385.